IOP Publishing | Royal Swedish Academy of Sciences Physica Scripta

Phys. Scr. **91** (2016) 104001 (6pp) doi:10.1088/0031-8949/91/10/104001

Atomistic simulations of the Fe *K*-edge EXAFS in FeF_3 using molecular dynamics and reverse Monte Carlo methods

Inga Jonane[1], Janis Timoshenko[2] and Alexei Kuzmin[1]

[1] Institute of Solid State Physics, University of Latvia, Kengaraga street 8, LV-1063 Riga, Latvia
[2] Physics Department, Yeshiva University, New York, NY 10016, USA

E-mail: a.kuzmin@cfi.lu.lv

Received 3 June 2016, revised 22 July 2016
Accepted for publication 27 July 2016
Published 17 August 2016

Abstract

Atomistic simulations of the experimental Fe *K*-edge extended x-ray absorption fine structure (EXAFS) of rhombohedral (space group $R\bar{3}c$) FeF_3 at $T = 300$ K were performed using classical molecular dynamics and reverse Monte Carlo (RMC) methods. The use of two complementary theoretical approaches allowed us to account accurately for thermal disorder effects in EXAFS and to validate the developed force-field model, which was constructed as a sum of two-body Buckingham-type (Fe–F and F–F), three-body harmonic (Fe–F–Fe) and Coulomb potentials. We found that the shape of the Fe *K*-edge EXAFS spectrum of FeF_3 is a more sensitive probe for the determination of potential parameters than the values of structural parameters (a, c, x(F)) available from diffraction studies. The best overall agreement between the experimental and theoretical EXAFS spectra calculated using *ab initio* multiple-scattering approach was obtained for the iron effective charge q(Fe) = 1.71. The RMC method coupled with the evolutionary algorithm was used for more elaborate analysis of the EXAFS data. The obtained results suggest that our force-field model slightly underestimates the amplitude of thermal vibrations of fluorine atoms in the direction perpendicular to the Fe–F bonds.

Keywords: iron fluoride, EXAFS, Fe K-edge, molecular dynamics, reverse Monte Carlo

(Some figures may appear in colour only in the online journal)

1. Introduction

Molecular dynamics (MD) and reverse Monte Carlo (RMC) methods are atomistic simulation techniques which allow one to accurately introduce the effects of static and thermal disorder into a calculation of extended x-ray absorption fine structure (EXAFS) within the multiple-scattering (MS) formalism. The MD simulation deals with a time-dependent 3D model of a material and provides a direct approach to EXAFS interpretation when the configuration-averaged EXAFS spectrum is evaluated from a set of atomic coordinates accumulated during the MD run and is compared with the experimental one. On the contrary, the RMC method solves an inverse problem thus reconstructing static atomic configuration from the experimental EXAFS data.

The application of MD and RMC methods to EXAFS has been known for several decades [1–4], however their use still remains rare on a routine basis due to large computational costs. Nevertheless, one can find many examples where these methods are applied to such complicated systems as nanoparticles [5–9]. Also, recent developments of the RMC method based on the implementation of so-called evolutionary algorithm [10] allowed one to reduce the needed computational time significantly, especially for EXAFS analysis of crystalline materials [11].

Analysis and interpretation of disorder effects in EXAFS in the presence of MS contributions is a challenging task [12–15] especially in perovskite-type materials whose structure contains linear or near-linear atomic chains leading to an increase of the MS signal amplitude [16–21]. Among many perovskites with the chemical formula ABX_3, there are some with A-place being vacant, for example, oxides ReO_3 and WO_3, oxyfluorides NbO_2F, TaO_2F, and $TiOF_2$, and several trifluorides ScF_3, TiF_3, VF_3, CrF_3, FeF_3 and GaF_3.

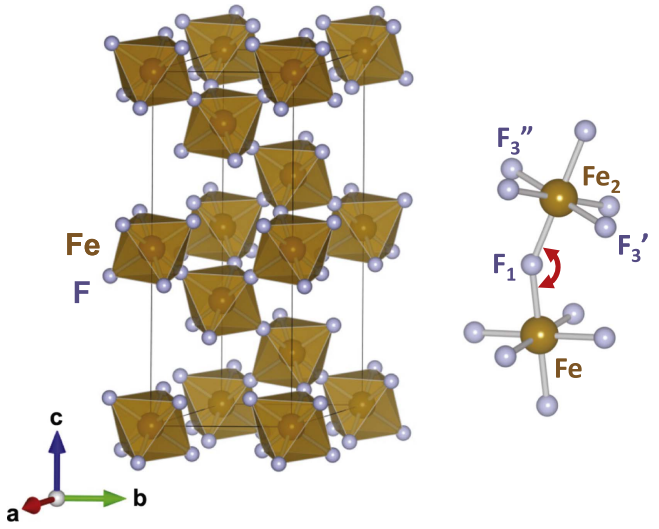

Figure 1. Crystalline structure of rhombohedral FeF_3 (space group $R\bar{3}c(167)$) [22, 23] and a fragment of FeF_3 structure showing connectivity between two adjacent FeF_6 octahedra. The bond angle Fe–F_1–Fe_2 and atoms (F_1, Fe_2, F_3) in the first three coordination shells around Fe are indicated. Note that the 24 fluorine atoms (F_3' and F_3'') in the third shell are split into two groups of 12 atoms each located at ~3.91 and ~4.46 Å.

The structure of iron trifluoride is built up of FeF_6 octahedra joined by vertices with iron atoms located at their centers (figure 1). It is often referred as VF_3-type and is derived from the cubic-ReO_3 structure by coupled rotations of the FeF_6 octahedra around one of the cubic body diagonals. The bond angle Fe–F–Fe between two adjacent octahedra is equal to ~153° [22, 23]. The deviation of fluorine atoms from linear chains reduces the symmetry of the crystal from cubic to rhombohedral with the space group $R\bar{3}c(167)$.

The practical interest in FeF_3 is driven by its perspective applications as a cathode in Li-ion batteries [24–29] and in catalysts [30–34]. FeF_3 is also a valuable compound for x-ray absorption spectroscopy studies due to its strong multiple-scattering contributions generated within atom chains –Fe–F–Fe–F–Fe– which leads to the so-called 'focusing' and 'super-focusing' effects [35].

In this study we demonstrate complementarity of molecular dynamics and reverse Monte Carlo simulations for a validation of the force-field models on the example of the analysis of the experimental Fe *K*-edge EXAFS of FeF_3 taken from [35].

2. MD-EXAFS simulations

The classical MD simulations were performed in the canonical (NVT) ensemble with periodic boundary conditions by the GULP4.2 code [36]. The simulation box was a rhombohedral $6a \times 6a \times 3c$ supercell containing 2592 atoms (648 irons and 1944 fluorines). The Newton's equations of motion were integrated with the Verlet leapfrog algorithm [37], with a time step of 0.5 fs. The Nosé–Hoover thermostat [38] was used to keep the average temperature around $T = 300$ K during simulations. After equilibration during 20 ps, a set of 4000 static atomic configurations was collected for the next 20 ps for each simulation run.

Our force-field model included two-body (Fe–F and F–F) and three-body (Fe–F–Fe) interactions as used previously for $LaCoO_3$ [21]. The two-body interactions were described by the potential [39] consisting of three terms

$$U_{ij}(r_{ij}) = A_{ij}\exp\left(-\frac{r_{ij}}{\rho_{ij}}\right) - \frac{C_{ij}}{r_{ij}^6} + \frac{q_i q_j e^2}{r_{ij}}. \quad (1)$$

The first two terms correspond to the Buckingham-type potential consisting of the Born–Mayer repulsive interaction between overlapping electron densities due to the Pauli principle and to the attractive van der Waals interaction, respectively. The last term describes the Coulomb interaction between pairs of ions having charges q_i and q_j.

The three-body interactions were accounted to reproduce the rhombohedral distortion and tilting motion of the FeF_6 octahedra. They were described by the harmonic potential [39]

$$U_{ijk} = \frac{1}{2}\kappa(\theta - \theta_0)^2, \quad (2)$$

where k is the force constant, and $\theta_0 = 152.53°$ is the equilibrium Fe–F–Fe bond angle.

The parameters (A, ρ, C and κ) of the force-field models for different values of the effective charge q(Fe) of iron ions are reported in table 1. The effective charge q(Fe) was varied from its formal value 3.0 down to 1.20. The charge of fluorine ions was calculated to maintain electroneutrality of the system as $q(\mathrm{F}) = -q(\mathrm{Fe})/3$.

The parameters (A, ρ, C and κ) were obtained for each value q(Fe) using the fitting procedure implemented in the GULP4.2 code [36]. The starting cell was constructed based on the structural parameters of FeF_3 obtained in time-of-flight neutron powder diffraction experiment [23] at $T = 300$ K and $P = 0.0001$ GPa: space group $R\bar{3}c$, $a = 5.198$Å, $c = 13.338$ Å and atoms occupying Wyckoff positions Fe $6b(0, 0, 0)$ and F $18e(x, 0.0, 3/4)$ with $x = -0.4122$. The parameters of the potential were fitted to the lattice parameters [23], the bulk modulus ($B_0 = 14$ GPa [23, 40]) and to three elastic constants ($C_{11} = 83.13$ GPa, $C_{22} = 98.64$ GPa and $C_{44} = 44.64$ GPa) calculated by first-principles calculations in [41]. The obtained force-field models were used to determine optimized values of structural parameters (a, c and x(F) in table 1) employed in the MD simulations.

Sets of static atomic configurations obtained in MD simulations were used to calculate configuration-averaged Fe *K*-edge EXAFS $\chi(k)$ (k is the photoelectron wavenumber) within the MS approach [42–44] by *ab initio* real-space MS FEFF8.50L code [13, 45].

The scattering potential and partial phase shifts were calculated within the muffin-tin (MT) approximation (15% overlap of the nearest MT-spheres [45]) only once for the cluster with the radius of 10 Å, centered at the absorbing Fe atom and constructed from the average atomic configuration, which corresponds to the crystallographic structure of FeF_3 [23].

Table 1. Force-field models and structural parameters for rhombohedral FeF_3 used in the molecular dynamics simulations.

	Experiment	q(Fe)					
	[23]	1.20	1.35	1.5	1.71	2.03	3.0
		Buckingham two-body potential Fe-F					
A (eV)		4094.09	6009.58	3812.55	3352.15	1962.56	991.978
ρ (Å)		0.239160	0.200221	0.199059	0.188788	0.187421	0.201106
		Buckingham two-body potential F-F					
A (eV)		13622.6	15422.6	14649.9	15977.4	16836.6	11665.7
ρ (Å)		0.235857	0.231639	0.230860	0.230019	0.228377	0.229524
C (eV Å^6)		85.5369	51.2790	41.0668	37.5132	33.6799	25.2836
		Three-body harmonic potential Fe-F-Fe					
κ (eV/rad^2)		0.18571	0.08541	0.06464	0.03705	0.04161	0.11739
θ_0 (°)		152.53	152.53	152.53	152.53	152.53	152.53
		Structural parameters					
a (Å)	5.1980	5.1935	5.1936	5.1927	5.1915	5.1871	5.1860
c (Å)	13.3380	13.3396	13.3396	13.3401	13.3399	13.3406	13.3439
x(F)	0.5878	0.5849	0.5851	0.5846	0.5835	0.5829	0.5765

Small variations of the cluster potential due to thermal vibrations during MD simulations were neglected. The MS contributions were accounted up to the 6th order to guarantee the convergence of the total EXAFS in the k-space range of interest. The photoelectron inelastic losses were accounted within the one-plasmon approximation using the complex exchange-correlation Hedin–Lundqvist potential [46]. The value of the amplitude reduction factor S_0^2 was set to 1.0 [13, 43].

The configuration-averaged Fe K-edge EXAFS $\chi(k)k^2$ spectra and their Fourier transforms (FTs) are shown in figure 2. The single-scattering (SS) and MS contributions to the total EXAFS $\chi(k)k^2$ spectra and their FTs are shown in figure 3 for the force-field model with q(Fe) = 1.71, which agrees best with the experimental data. Note that this value of the effective charge is not far from the value of Bader charge (q(Fe) = 2.03) calculated in [41] using the plane-wave density functional theory (DFT). The total and partial radial distribution functions (RDFs) $G(R)$ obtained from the MD simulations are reported in figure 4.

3. Reverse Monte Carlo simulations

The RMC method coupled with the evolutionary algorithm (EA) has been described by us in detail in [11] and allows us to obtain a 3D structure model of FeF_3, consistent with the experimental Fe K-edge EXAFS.

The structure of FeF_3 was simulated as an infinite crystal with the periodic boundary conditions based on supercells consisting of $4a \times 4a \times 2c$ or $8a \times 8a \times 4c$ elementary cells (including 768 or 6144 atoms, respectively), which were constructed using the diffraction data from [23].

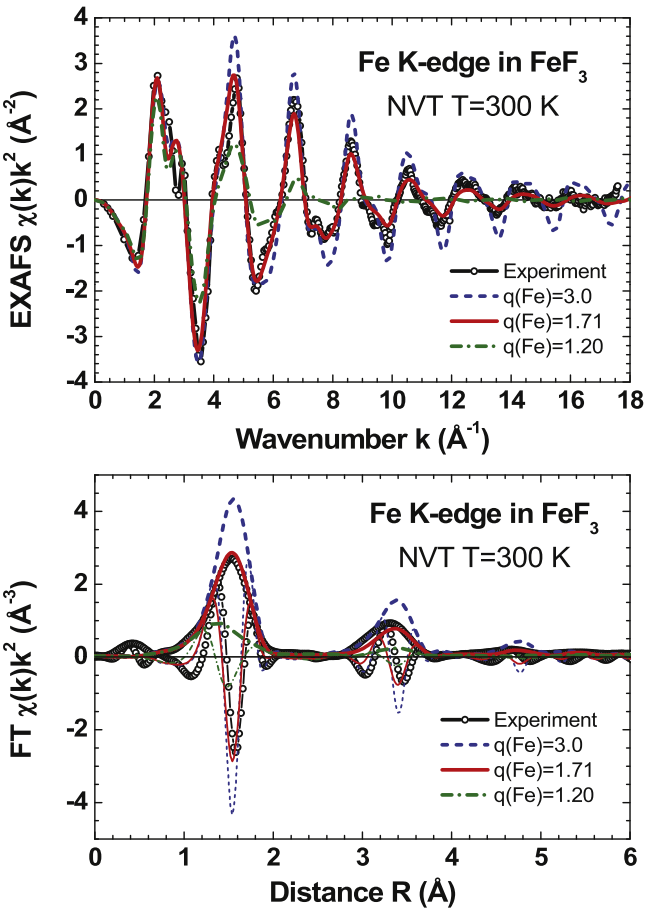

Figure 2. A comparison of the experimental [35] and calculated Fe K-edge MD-EXAFS $\chi(k)k^2$ spectra and their Fourier transforms (FTs) (modulus and imaginary parts are shown) in FeF_3 at T = 300 K. Only few spectra calculated for different effective iron charges are shown for clarity.

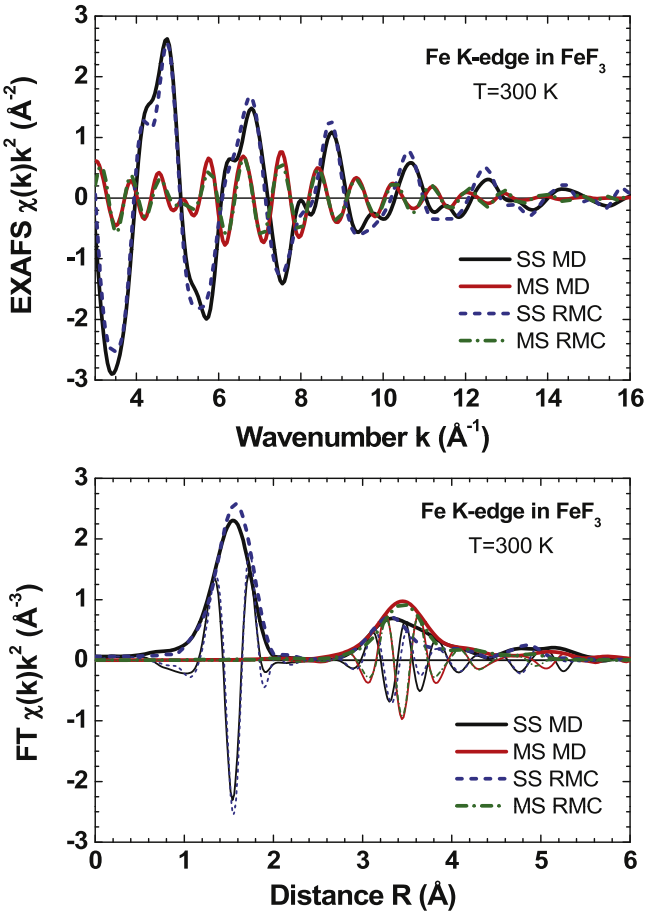

Figure 3. A sum of the single-scattering (SS) and multiple-scattering (MS) contributions to the Fe *K*-edge MD-EXAFS (for $q(\mathrm{Fe}) = 1.71$) and RMC/EA-EXAFS $\chi(k)k^2$ spectra and their Fourier transforms (FTs) (modulus and imaginary parts are shown) for FeF_3 at $T = 300$ K.

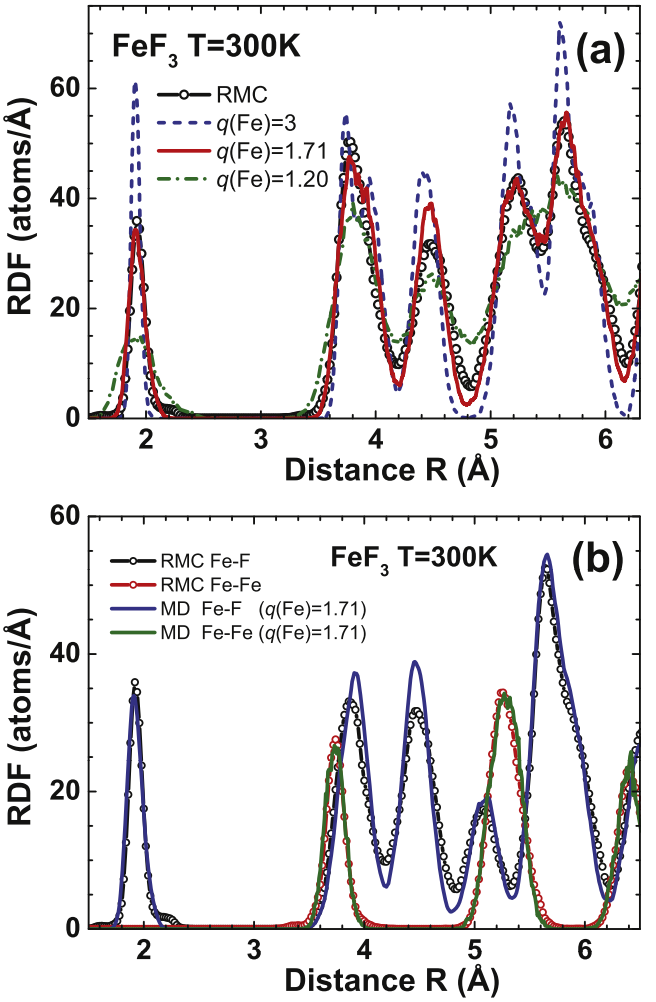

Figure 4. Total (a) and partial (b) radial distribution functions (RDFs) $G(R)$ calculated from the results of the MD and RMC simulations for FeF_3 at $T = 300$ K.

RMC/EA calculations were performed for 64 atomic configurations simultaneously. A new atomic configuration was generated by randomly moving all atoms in the supercell within the allowed maximal displacement of 0.4 Å. Configuration-averaged theoretical EXAFS spectra were calculated by *ab initio* self-consistent real-space MS FEFF8.50L code [13, 45], taking into account contributions from the MS effects as in section 2. After each iteration the experimental and calculated Fe *K*-edge EXAFS spectra were compared using Morlet wavelet transform (WT) [47] in the *k*-space range from 3.5 to 16 Å^{-1} and in the *R*-space range from 1 to 5 Å. After 6000 iterations there was no improvement in the agreement between the experimental and simulated EXAFS data.

The result of RMC/EA-EXAFS calculations of the Fe *K*-edge EXAFS spectrum for FeF_3 is shown in figure 5. Note that the difference between the experimental and calculated EXAFS spectra is almost negligible.

Separate contributions of the SS and MS effects into the EXAFS spectrum are shown in figure 3 and the partial RDFs for Fe–F and F–F atom pairs are reported in figure 4. The final atomic configuration was used to determine a number of useful structural parameters such as radial and bond-angle distribution functions, average interatomic distances and mean-square relative displacements (MSRD).

4. Results and discussion

A comparison of partial SS and MS contributions into the total Fe *K*-edge EXAFS of FeF_3 obtained using MD-EXAFS and RMC/EA-EXAFS simulations is shown in *k* and *R*-space in figure 3. As one can see, both methods give rather close results that indicate on the similarity of underlying atomic structure. Also the significant MS contribution in the range of the second peak in FT at 3.5 Å is well observed in both simulations, as was expected from previous studies [35, 48].

The average interatomic distances and MSRD factors for the first two coordination shells obtained by both methods are reported in table 2. To evaluate the uncertainties of obtained results, RMC/EA calculations were performed several times with different sequences of pseudo-random numbers [11]. Note that the values of our interatomic distances agree well with those obtained by diffraction, 1.922 Å for Fe–F_1 and 3.735 Å for Fe–Fe_2 atom pairs in [23].

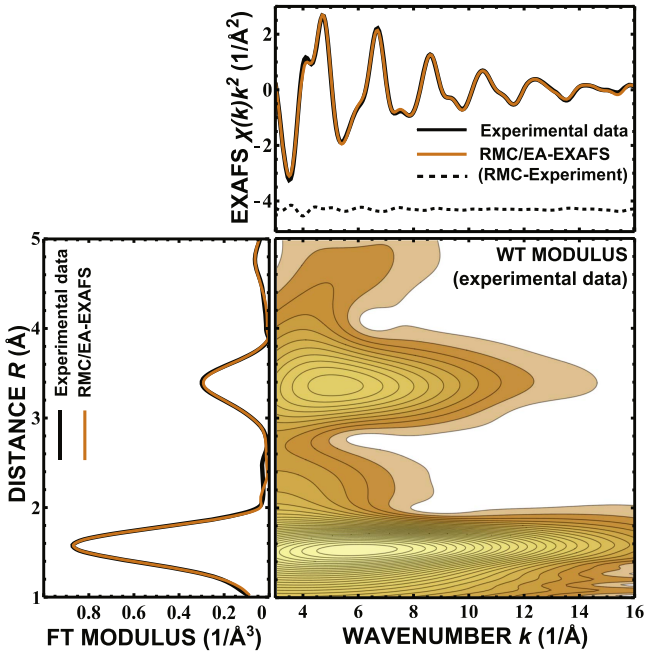

Figure 5. Results of RMC/EA-EXAFS calculations for FeF_3 at $T = 300$ K. Upper panel: a comparison of the experimental and calculated Fe K-edge EXAFS spectra $\chi(k)k^2$ and their difference. Bottom left panel: the Fourier transforms of the EXAFS spectra shown in the upper panel. Bottom right panel: the wavelet transform of the experimental EXAFS spectrum.

Table 2. Average interatomic distances (R) and MSRD factors (σ^2) for the first two coordination shells (Fe–F_1 and Fe–Fe_2 atom pairs) obtained by the MD and RMC/EA simulations.

	R_{MD} (Å)	$R_{RMC/EA}$ (Å)	σ^2_{MD} (Å^2)	$\sigma^2_{RMC/EA}$ (Å^2)
Fe–F_1	1.927	1.938 ± 0.005	0.0055	0.004 ± 0.001
Fe–Fe_2	3.734	3.739 ± 0.005	0.0072	0.008 ± 0.001

Detailed comparison of two model EXAFS spectra indicates, however, some difference between them, which can be understood from the analysis of partial RDFs $G(R)$ in figure 4(b). While the Fe–Fe RDFs (peaks at ~3.7 Å and ~5.2 Å) are close, some difference is clearly present in the Fe–F RDFs at ~1.93 Å and, especially, at ~3.91 Å and ~4.46 Å. The first difference is due to that in the values of the MSRD factors σ^2(Fe–F_1) in the first coordination shell of iron (figure 1), reported in table 1 and related to the correlated motion of iron and fluorine atoms parallel to the Fe–F bonds. The next two peaks in the Fe–F RDFs are due to 12 F_3' and 12 F_3'' atoms (figure 1), which are separated due to the tilting of FeF_6 octahedra. Note that differently to the F_1 atoms, the vibrations of F_3 atoms, seen from the central Fe atom, correspond to large extent to the fluorine atom motion perpendicular to the Fe–F bonds. Therefore, the observed difference in the MSRD of Fe–F_3 atom pairs indicates that the force-field models reported in table 1 fail to reproduce accurately the tilting motion of FeF_6 octahedra.

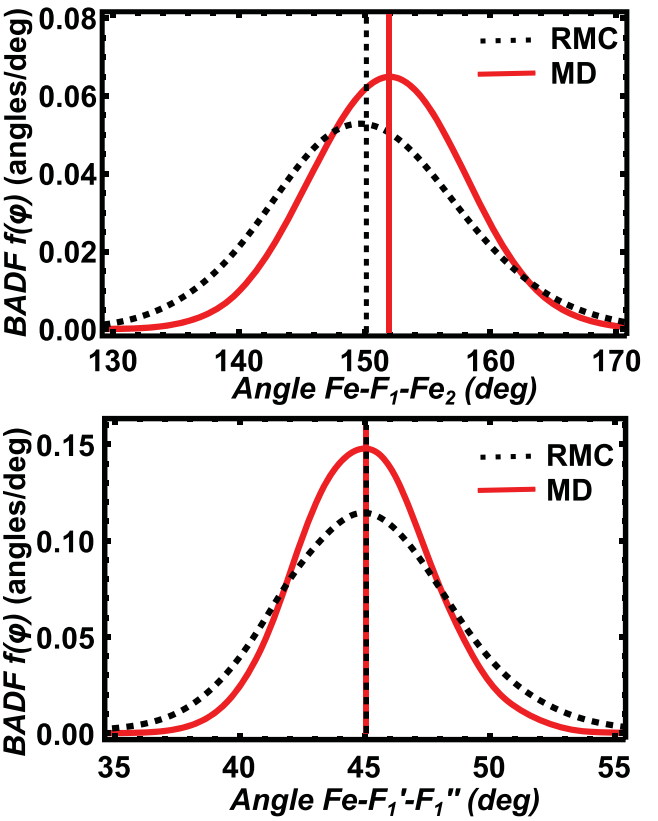

Figure 6. Bond-angle distribution function (BADF) for Fe–F_1–Fe_2 and Fe–F_1'–F_1'' angles, obtained by MD and RMC/EA simulations. Vertical lines show the mean values of the BADFs.

Finally, we compare bond-angle distribution functions (BADFs) obtained from MD and RMC/EA simulations for Fe–F_1–Fe_2 and Fe–F_1'–F_1'' (F_1' and F_1'' are two different neighbouring fluorine atoms in the first shell of iron) angles in figure 6. Smaller mean value of the bond angle Fe–F_1–Fe_2 obtained by MD correlates with smaller amplitude of FeF_6 octahedra tilting motion discussed above. The distribution of the Fe–F_1'–F_1'' angle characterizes the rigidity of FeF_6 octahedra and is symmetric in both cases. However, it is slightly narrower in the case of the MD model.

5. Conclusions

In this study we performed atomistic simulations of the experimental Fe K-edge extended x-ray absorption fine structure of rhombohedral (space group $R\bar{3}c$) FeF_3 at $T = 300$ K [35] using two complementary approaches—molecular dynamics (MD) and reverse Monte Carlo (RMC) methods.

A simple force-field model was developed for FeF_3 taking into account two-body (Fe–F and F–F) and three-body (Fe–F–Fe) interactions by fitting to the experimental values of the lattice parameters and bulk modulus as well as to the calculated values of three elastic constants.

We found that different sets of the potential parameters corresponding to the iron effective charge q(Fe) in the range

from 1.20 to 3.0 are compatible with the experimental values of structural parameters (a, c, x(F)) for FeF_3. To resolve this ambiguity, classical MD simulations of the Fe K-edge EXAFS were performed in the canonical (NVT) ensemble at $T = 300$ K using *ab initio* multiple-scattering approach, and the best overall agreement was obtained for q(Fe) = 1.71. To understand the origin of the remaining small discrepancy, the EXAFS was simulated by the RMC method coupled with the evolutionary algorithm. A comparison of the radial distribution functions for the Fe–F and Fe–Fe atom pairs, determined from the MD and RMC simulations, indicates that our force-field model underestimates slightly the amplitude of thermal vibrations of fluorine atoms in the direction perpendicular to the Fe–F bonds.

Acknowledgments

The work was supported by the Latvian Science Council Grant no. 187/2012.

References

[1] Gurman S J and McGreevy R L 1990 *J. Phys.: Condens. Matter* **2** 9463–73
[2] D'Angelo P, Di Nola A, Filipponi A, Pavel N and Roccatano D 1994 *J. Chem. Phys.* **100** 985–94
[3] Palmer B J, Pfund D M and Fulton J L 1996 *J. Phys. Chem.* **100** 13393–8
[4] Winterer M 2000 *J. Appl. Phys.* **88** 5635–44
[5] Roscioni O M, Zonias N, Price S W, Russell A E, Comaschi T and Skylaris C K 2011 *Phys. Rev.* B **83** 115409
[6] Anspoks A, Kalinko A, Kalendarev R and Kuzmin A 2012 *Phys. Rev.* B **86** 174114
[7] Tupy S A, Karim A M, Bagia C, Deng W, Huang Y, Vlachos D G and Chen J G 2012 *ACS Catal.* **2** 2290
[8] Kompch A, Sahu A, Notthoff C, Ott F, Norris D J and Winterer M 2015 *J. Phys. Chem.* C **119** 18762–72
[9] Timoshenko J, Anspoks A, Kalinko A and Kuzmin A 2015 *Phys. Stat. Sol.* A **212** 265–73
[10] Holland J H 1992 *Adaptation in Natural and Artificial Systems: an Introductory Analysis with Applications to Biology, Control, and Artificial Intelligence* (Cambridge, MA: MIT Press)
[11] Timoshenko J, Kuzmin A and Purans J 2014 *J. Phys.: Condens. Matter* **26** 055401
[12] Filipponi A, Di Cicco A and Natoli C R 1995 *Phys. Rev.* B **52** 15122–34
[13] Rehr J J and Albers R C 2000 *Rev. Mod. Phys.* **72** 621–54
[14] Ravel B 2005 *J. Alloys Compd.* **401** 118–26
[15] Di Cicco A and Trapananti A 2005 *J. Phys.: Condens. Matter* **17** S135
[16] Kuzmin A, Purans J, Benfatto M and Natoli C R 1993 *Phys. Rev.* B **47** 2480–6
[17] Kuzmin A and Purans J 1993 *J. Phys.: Condens. Matter* **5** 267–82
[18] Krayzman V, Levin I and Tucker M G 2008 *J. Appl. Crystallogr.* **41** 705–14
[19] Krayzman V, Levin I, Woicik J C, Proffen T, Vanderah T A and Tucker M G 2009 *J. Appl. Crystallogr.* **42** 867–77
[20] Vailionis A, Boschker H, Siemons W, Houwman E P, Blank D H A, Rijnders G and Koster G 2011 *Phys. Rev.* B **83** 064101
[21] Kuzmin A, Efimov V, Efimova E, Sikolenko V, Pascarelli S and Troyanchuk I O 2011 *Solid State Ion.* **188** 21–4
[22] Leblanc M, Pape R D, Ferey G and Pannetier J 1986 *Solid State Commun.* **58** 171–6
[23] Jørgensen J E and Smith R I 2006 *Acta Crystallogr.* B **62** 987–92
[24] Zhou M, Zhao L, Doi T, Okada S and Yamaki J 2010 *J. Power Sources* **195** 4952–6
[25] Kim S W, Seo D H, Gwon H, Kim J and Kang K 2010 *Adv. Mater.* **22** 5260–4
[26] Ma R, Wang M, Tao P, Wang Y, Cao C, Shan G, Yang S, Xi L, Chung J C Y and Lu Z 2013 *J. Mater. Chem.* A **1** 15060–7
[27] Li C, Mu X, van Aken P A and Maier J 2013 *Adv. Energy Mater.* **3** 113–9
[28] Tan J *et al* 2014 *J. Power Sources* **251** 75–84
[29] Bai Y, Zhou X, Jia Z, Wu C, Yang L, Chen M, Zhao H, Wu F and Liu G 2015 *Nano Energy* **17** 140–51
[30] Yavari A, LeMoulec A, de Castro F, Deledda S, Friedrichs O, Botta W, Vaughan G, Klassen T, Fernandez A and Kvick Å 2005 *Scr. Mater.* **52** 719–24
[31] Surasani R, Kalita D, Rao A D, Yarbagi K and Chandrasekhar K 2012 *J. Fluorine Chem.* **135** 91–6
[32] Bhaskar Kumar T, Sumanth C, Dhanunjaya Rao A V, Kalita D, Srinivasa Rao M, Chandra Sekhar K B, Shiva Kumar K and Pal M 2012 *RSC Adv.* **2** 11510–9
[33] Nehme G 2012 *Trib. Trans.* **55** 829–45
[34] Guo Y, Gaczynski P, Becker K D and Kemnitz E 2013 *Chem. Cat. Chem* **5** 2223–32
[35] Kuzmin A and Parent P 1994 *J. Phys.: Condens. Matter* **6** 4395–404
[36] Gale J D and Rohl A L 2003 *Mol. Simul.* **29** 291–341
[37] Hockney R W 1970 *Methods Comput. Phys.* **9** 135–211
[38] Hoover W G 1985 *Phys. Rev.* A **31** 1695–7
[39] Gale J D 1996 *Phil. Mag.* B **73** 3–19
[40] Zhu F, Lai X, Wu X, Li Y and Qin S 2014 *Acta Crystallogr.* B **70** 801–8
[41] Ma Y, Lockwood G K and Garofalini S H 2011 *J. Phys. Chem.* C **115** 24198–205
[42] Kuzmin A and Evarestov R A 2009 *J. Phys.: Condens. Matter* **21** 055401
[43] Kuzmin A and Chaboy J 2014 *IUCrJ* **1** 571–89
[44] Kuzmin A, Anspoks A, Kalinko A and Timoshenko J 2016 *Z. Phys. Chem.* **230** 537–49
[45] Ankudinov A L, Ravel B, Rehr J J and Conradson S D 1998 *Phys. Rev.* B **58** 7565–76
[46] Hedin L and Lundqvist S 1971 *J. Phys. C: Solid State Phys.* **4** 2064
[47] Timoshenko J, Kuzmin A and Purans J 2012 *Comp. Phys. Commun.* **183** 1237–45
[48] Kuzmin A, Purans J and Parent P 1995 *Physica* B **208-209** 45–6